



**HAL**  
open science

## A pavement-watering thermal model for SOLENE-microclimat: development and evaluation

Marie-Hélène Azam, Jérémy Bernard, Benjamin Morille, Marjorie Musy,  
Hervé Andrieu

► **To cite this version:**

Marie-Hélène Azam, Jérémy Bernard, Benjamin Morille, Marjorie Musy, Hervé Andrieu. A pavement-watering thermal model for SOLENE-microclimat: development and evaluation. *Urban Climate*, 2018, 25, pp.22 - 36. 10.1016/j.uclim.2018.04.005 . hal-01790917v1

**HAL Id: hal-01790917**

**<https://hal.science/hal-01790917v1>**

Submitted on 14 May 2018 (v1), last revised 31 May 2018 (v2)

**HAL** is a multi-disciplinary open access archive for the deposit and dissemination of scientific research documents, whether they are published or not. The documents may come from teaching and research institutions in France or abroad, or from public or private research centers.

L'archive ouverte pluridisciplinaire **HAL**, est destinée au dépôt et à la diffusion de documents scientifiques de niveau recherche, publiés ou non, émanant des établissements d'enseignement et de recherche français ou étrangers, des laboratoires publics ou privés.

# A pavement-watering thermal model for SOLENE-microclimat: development and evaluation

AZAM Marie-Hélène<sup>a,c,1,\*</sup>, BERNARD Jérémy<sup>b</sup>, MORILLE Benjamin<sup>a</sup>,  
MUSY Marjorie<sup>a,c,1</sup>, ANDRIEU Hervé<sup>a,d</sup>

<sup>a</sup>*Institut de Recherche en Sciences et Techniques de la Ville, FR CNRS 2488, F-44000  
Nantes, France*

<sup>b</sup>*UMR CNRS 6285, Lab-STICC, F-56000 Vannes, France*

<sup>c</sup>*Cerema, F-44000 Nantes, France*

<sup>d</sup>*Institut français des sciences et technologies des transports, de l'aménagement et des  
réseaux, F-44000 Bouguenais, France*

<sup>e</sup>*UMR CNRS 6183, GeM, Université de Nantes, F-44000 Nantes, France*

---

## Abstract

In a dense urban area, pavement watering could be a solution to mitigate the Urban Heat Island. For now, mainly experimental studies have been used to evaluate watering techniques. In this study, a soil model dedicated to pavement watering has been developed within the urban climate model SOLENE-Microclimat. This watering model is presented and evaluated via a measurement campaign performed on an asphalt car park during hot days. The measurements campaign reveals that the surface cooling is mainly due to evaporation (80%). However, under warm conditions, the heat flux exchanged between the runoff water and the surface should also be modelled. Indeed, watering events are modelled through a runoff convective heat flux and a latent heat flux. The mean daily RMSE between estimated and observed surface temperature is 1.04°C, 0.86°C, 0.66°C, 0.35°C and 0.21°C

---

\*Corresponding author. E-mail address: marie-helene.azam@cerema.fr Address: Cerema, 9 rue René Viviani, 44000 Nantes, France

respectively at the surface, 5 cm-, 10 cm-, 34 cm- and 50 cm-depths.

*Keywords:* Pavement-watering, Soil surface temperature,  
SOLENE-Microclimat, Urban Heat Island, Climate Adaptation

---

## Highlights

- A watering model is proposed to assess the impact of pavement watering techniques.
- Waterings are modelled through a runoff convective heat flux and a latent heat flux.
- Under warm condition both fluxes should be modelled to reproduce the dynamics.
- Temperature observed at several depths are used to evaluate the computed temperature.

## Contents

<b>1</b>	<b>Introduction</b>	<b>4</b>
1.1	Watering techniques . . . . .	4
1.2	Pavement watering in microclimatic models . . . . .	5
<b>2</b>	<b>Method</b>	<b>7</b>
2.1	SOLENE-microclimat soil model . . . . .	8
2.2	Proposed watering model . . . . .	9
2.2.1	Energy balance at the surface . . . . .	9
2.2.2	Runoff convective heat flux . . . . .	11
2.2.3	Latent heat flux between water and atmosphere . . . . .	11
2.2.4	Heat fluxes dynamic . . . . .	15
<b>3</b>	<b>Model assessment</b>	<b>16</b>
3.1	The campaign and the data . . . . .	16
3.1.1	Studied area and measurement description . . . . .	16
3.1.2	Description of the watering events . . . . .	18
3.1.3	Consistency of the heat fluxes dynamics with the model assumptions . . . . .	19
3.1.4	Water budget . . . . .	22
3.2	Comparison between simulation and measurement . . . . .	23
3.2.1	Model setup . . . . .	23
3.2.2	Watering model evaluation on ROSURE data . . . . .	26
3.2.3	Model's sensitivity to the discretization . . . . .	30
<b>4</b>	<b>Conclusion</b>	<b>32</b>

## 1. Introduction

The Intergovernmental Panel on Climate Change (IPCC) assessed that heatwaves will be more frequent and more intense during the 21<sup>st</sup> century than during the 20<sup>th</sup> century. The last major European heatwaves led to approximately 70,000 excess deaths across the continent (Robine et al., 2008 [1]). The urban heat island (hereafter denoted UHI) effect exacerbates the consequences of such climatic event on human health, as confirmed by Laaidi et al. (2012 [2]) and Conti et al. (2005 [3]) who showed a clear relationship between UHI and mortality respectively in Paris and in Italian cities. Reducing the UHI is then a major challenge addressed to the scientist community. Several countermeasures are currently investigated in all regions of the world and under different climates. Santamouris et al. (2016 [4]) performed a review of the performances of the most common UHI mitigation technologies: building material albedo, vegetation, water. He concludes that UHI may be partly or fully annihilated using a combination of all technologies but that there is a need to improve the performances of each of them. The present article focuses on the pavement watering solution. The correct modeling of the physical phenomenon induced by this technique and their interaction with local climate will help to improve its performances.

### 1.1. Watering techniques

In very dense urban areas, the UHI may be mitigated spreading water over pavements. The evaporation of the water in the air and the heat flux exchanged between the water and the ground contribute to cool both the surface and the air temperature. Under warm conditions, these processes

25 offer a quick response while the water is spread over the surface. However, the  
26 evaporation is constrained by the pavement water-holding capacity (which  
27 depends on the surface roughness). Below a certain volume of water spread,  
28 all the water is stored in the surface porosity and can evaporate. Above a  
29 threshold proper to the surface characteristics, the holding capacity of the  
30 surface is overpassed and the water excess streams toward sewers.

31 Watering techniques have been mainly studied through experimental works  
32 (Hendel et al., 2015 [5], Himeno et al., 2010 [6]) which confirm the positive  
33 impact of watering technique. Himeno et al., (2010 [6]) found that in the case  
34 of hot weather (above 30°C), pavement watering can reduce the air tempera-  
35 ture to 2°C in the morning and 4°C in the afternoon. Hendel et al. (2015 [7])  
36 work on the optimization of those waterings, minimizing the total amount  
37 of water spread, maximizing the evaporation. With a watering rate of 0.31  
38 to 0.41L/m<sup>2</sup>/h every 30 minutes, the surface temperature could be reduced  
39 to 4°C in the morning and 13°C in the afternoon. According to Broadbent  
40 et al. (2017 [8]), the performance assessment of watering techniques during  
41 heatwave conditions at the microscale has rarely been modelled. Daniel et  
42 al. (2016 [9]), Grossman-Clarke et al. (2010 [10]) and Boadbent et al. (2017  
43 [8]) evaluated the mitigation potential of these techniques at the mesoscale.

#### 44 *1.2. Pavement watering in microclimatic models*

45 In the literature, most of the tools used to simulate the urban surface  
46 energy balance, calculate the latent heat flux induced by the vegetation  
47 (Grimmond et al., 2010 [11]). However, theirs models are not appropriate  
48 for pavement watering application since they do not consider the heat flux

49 exchanged between the surface and the runoff water.

50 The Town Energy Balance (TEB) model (Masson, 2000 [12]) is one of  
51 the few urban climate models that is able to simulate pavement watering  
52 events (Daniel et al., 2016 [9], Broadbent et al. (2017 [8]) at mesoscale. It  
53 distinguishes the evapotranspiration from the evaporation over impervious  
54 surfaces. In the case of impervious surface, the following processes are mod-  
55 elled: interception, evaporation of the available water and surface runoff. For  
56 each surface, a water reservoir is set according to the water holding capacity  
57 of the pavement and its content is updated at each time step. It is filled dur-  
58 ing a watering event and emptied by the evaporation. When the maximum  
59 capacity of the reservoir is reached, the excess is transferred to the sewer.  
60 By default, the pavement considered in the model is a road and its storage  
61 capacity is set at 1mm (Daniel et al., 2016 [9]). However, this parameter is  
62 a variable of the model and then may be set to a different value (see section  
63 3.2.1).

64 The main purpose of this article is to present and evaluate a watering  
65 model that has been developed within the SOLENE-Microclimat model. This  
66 microclimatic model is a research tool dedicated to urban climate modeling  
67 at the neighborhood scale. It consists of several model pieces including a  
68 radiative model SOLENE, and several urban surfaces models (buildings, soils,  
69 vegetation...) which have been described and assessed in (Malys, 2012 [13];  
70 Musy, 2015 [14]; Bouyer et al., 2011 [15]). In this tool as in most of the  
71 microclimate tools (Grimmond et al., 2010 [11]), waterings over impervious  
72 surface could not be model.



73 The watering model is elaborated based on a review of the literature and  
74 evaluated on an open asphalt parking lot, chosen to avoid interferences with  
75 other surfaces thermal behavior, like solar radiation diffusion and reflection as  
76 well as long-wave emission from the surrounding vertical surfaces (building  
77 facades). In these conditions, we can isolate the watering model from the  
78 other SOLENE-microclimat model pieces and assess it properly. This article  
79 is the second step of a complete evaluation of SOLENE-Microclimat soil  
80 model. Indeed in a previous article (Azam et al., 2017 [16]), the soil model  
81 has been assessed under same conditions.

82 The model is first presented in section 2. After a review of the different  
83 methods used to calculate each heat flux, the equations used in the model  
84 are developed and the algorithm is sum-up in a flow-chart (section 2.2.4). In  
85 section 3, the model is assessed. The measurement campaign used is first  
86 presented (section 3.1). Based on those results assumptions previously made  
87 are verified. Results of the model are compared to the observed temperature  
88 and heat flux (section 3.2). The model is evaluated on the surface tempera-  
89 ture and latent heat flux calculation. Finally, the sensitivity of the model to  
90 the soil model node distribution is studied.

## 91 **2. Method**

92 The proposed watering pavement model will be an additional model pieces  
93 to the soil model used in SOLENE-microclimat. The SOLENE-microclimat  
94 original soil model is briefly presented in section 2.1 but further details are  
95 available in Azam et al.(2017 [16]). Then the proposed watering model is  
96 presented in section 2.2.

97 *2.1. SOLENE-microclimat soil model*

98 SOLENE-microclimat soil model is designed for an impervious surface  
 99 like a pavement coating. Only heat transfer is therefore taken into account,  
 100 the moisture transfer being neglected. The soil model is defined as a one-  
 101 dimensional soil column (for each soil facet) where each layer has its own  
 102 characteristics (Figure 1)

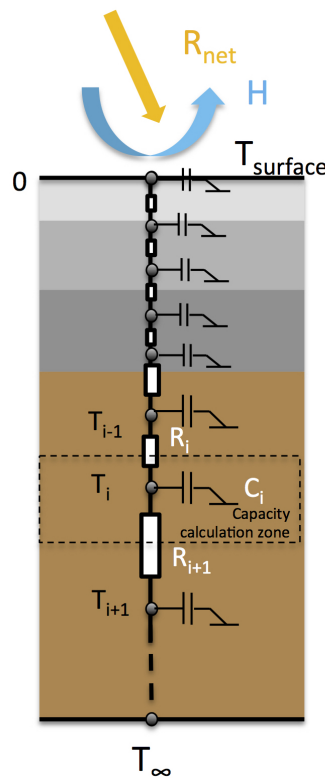


Figure 1: Schematic representation of the soil model: representation of node distribution, heat resistances and capacities, description of a common cross-section of urban soil column with diffusive materials layers in shade of gray and underneath natural soil in brown (Azam et al., 2017 [16])

103 The problem is solved by a finite difference method using an electrical

104 analogy. A mesh with one node per centimeter is used. At the surface,  
105 the upper boundary condition is defined by the surface energy balance detail  
106 after. The temperature at 0.75m is set with the measured temperature signal  
107 at this depth. A more detailed description of the SOLENE-microclimat soil  
108 model can be found in (Azam et al., 2017 [16]).

## 109 *2.2. Proposed watering model*

### 110 *2.2.1. Energy balance at the surface*

111 The net radiative heat flux density ( $R_{net}$ ) that reaches a dry pavement  
112 is transformed in two fluxes: a conductive heat flux density ( $Q_{cond}$ ) and a  
113 sensible heat flux density ( $H$ ). Equation (1) is used to define the upper  
114 boundary condition of the soil model.

$$R_{net} = Q_{cond} + H \quad (1)$$

115

116  $R_{net}$ : net radiative heat flux density [ $W/m^2$ ]

117  $Q_{cond}$ : conductive heat flux density [ $W/m^2$ ]

118  $H$ : sensible heat flux density [ $W/m^2$ ]

119

120 A watering event alters this energy balance. The water spread on a surface  
121 follows one of the following path: 1/ infiltration in the soil, 2/run-off toward  
122 the neighboring surface or to the water network and 3/evaporation. Each  
123 path implies a modification of the surface energy balance:

- 124 • a part of the water infiltrates the soil: the thermal properties of the soil  
125 can vary with the water content and a heat flux is exchanged between

126 the water and the soil layers.

127 • a part of the water runs-off: a heat flux is exchanged between the water  
128 and the surface.

129 • a part of the water evaporates: a latent heat flux is exchanged between  
130 the water and the atmosphere.

131 Pavement surfaces can be modelled as semi-impervious surfaces (Dupont et  
132 al., 2006 [17]) or as impervious surfaces (Herb et al., 2008 [18]; Hendel et al.,  
133 2015 [7]). In the first case, downward infiltration should be taken into account  
134 whereas the proportion of infiltrated water in the second case is supposed  
135 negligible compared with the one that runs-off or evaporates. In this study,  
136 we will consider our surface as impervious. Overall the watering model needs  
137 to take into account two fluxes initially not considered in Equation (1): a  
138 runoff convective heat flux density exchanged between the surface and the  
139 water ( $Q_{wat-pav}$ ) and a latent heat flux density ( $LE$ ) between the water and  
140 the atmosphere (Herb et al., 2008 [18]; Hendel et al., 2015 [7]). The resulting  
141 surface energy balance is then given by Equation (2). The calculation of  
142 these fluxes is further described in the following sections.

$$R_{net} = Q_{cond} + H + Q_{wat-pav} + LE \quad (2)$$

143

144  $LE$ : latent heat flux density exchanged between the water and the atmo-  
145 sphere [ $W/m^2$ ]

146  $Q_{wat-pav}$ : runoff convective heat flux density exchanged between the surface  
147 and the water [ $W/m^2$ ]

148

149 *2.2.2. Runoff convective heat flux*

150 Herb et al. (2008 [18]) estimate the convective heat flux exchanged be-  
151 tween the surface and the water from the energy absorbed the water and  
152 released by the soil. With the same idea, in our model, this runoff convective  
153 flux is calculated from the energy absorbed by the water (Equation (3)). The  
154 temperature variation is calculated between the soil surface temperature at  
155  $t$  and the temperature of the water before it touches the ground. Herb et al.  
156 (2008 [18]) model rain events, the water temperature is then supposed equal  
157 to the dew-point temperature. In our case, the water spread is suppose equal  
158 to the water system temperature.

$$Q_{wat-pav} = \frac{\rho_w \cdot C_{p,w} \cdot h_{w,spr}}{\Delta t} (T_{surf}(t) - T_w) \quad (3)$$

159

160  $h_{w,spr}$ : water height evenly sprinkled on the surface [ $m$ ]

161  $T_w$ : temperature of the water [ $K$ ]

162  $\rho_w$ : water density [ $kg/m^3$ ]

163  $C_{p,w}$ : water specific heat [ $J/kg/K$ ]

164

165 Herb et al. (2008 [18]) made the assumption that the runoff water reaches  
166 the ground temperature instantly by conduction. The same assumption will  
167 be made in the model and verified from the measurements analysis in section  
168 3.1.3.

169 *2.2.3. Latent heat flux between water and atmosphere*

170 The evaporation is driven by two factors: the amount of heat available  
171 at the free surface and the vapor pressure gradient in the near air. These

172 factors depend on meteorological variables including radiation, air pressure,  
 173 wind speed, temperature but also on other variables like the surface rugosity.  
 174 Various methods have been developed to evaluate the evaporation rate. Xu  
 175 and Singh (1997 [19]; 2001 [20]) proposed to sort them into 6 classes: (i)  
 176 water budget, (ii) mass-transfer or aerodynamic based method, (iii) energy  
 177 budget method or combination (e.g. Penman, 1948), (iv) radiation, (v) tem-  
 178 perature based method, (vi) empirical methods. The empirical methods are  
 179 applicable for only a limited range of cases or parameters, which makes them  
 180 not applicable to our case. Singh and Xu (1997 [19]) observed that the water  
 181 budget methods are based on a simple theoretical basis but that they rarely  
 182 produce reliable results. The energy budget methods and the combination  
 183 method reproduce well the physics but they need a considerable amount of  
 184 meteorological input data. The mass-transfer method is a good compromise  
 185 since the accuracy is reasonable (Singh and Xu, 1997 [19]) for a less meteoro-  
 186 logical input data needed. For this reason, it is the method most commonly  
 187 used by researchers to develop soil models (Asaeda and Ca, 1993 [21]; Qin et  
 188 al., 2002 [22]; Saito and Simunek, 2009 [23]; Herb et al., 2008 [18], Best, 1998  
 189 [24]). It is also used in our model.

190 The mass-transfer method is based on the Dalton Equation, described by  
 191 Equation (4).

$$LE = C \cdot [q_{sat}(T_{surf}) - q_a(T_{air})] \quad (4)$$

192

193  $C$ : the aerodynamic conductance

194  $q_{sat}(T_{surf}) - q_a(T_{air})$ : the vapor pressure gradient between the actual air va-

195 por pressure and the saturation vapor pressure at the surface temperature

196

197 The aerodynamic conductance is generally modelled using a combination  
198 of the air density  $\rho_{air}$ , the latent heat  $L$ , and a heat transfer resistance  $R$   
199 (Equation (5)). Several method can be used to calculate this last parameter.  
200 The heat transfer resistance can be calculated as a function of the convective  
201 heat transfer coefficient  $h_c$  ( Mihalakakou et al. 1997 [25]; Herb et al., 2008  
202 [18]); or as a combination of a surface and an aerodynamic resistance cal-  
203 culated using standard Monin-Obukhov similarity theory (Best, 1998 [24];  
204 Asaeda and Ca, 1993 [21]; Qin et al., 2002 [22]; Saito and Simunek, 2009  
205 [23]).

$$C = \rho_{air} \cdot \frac{L}{R} \quad (5)$$

206

207  $\rho_{air}$ : air density [ $kg/m^3$ ]

208  $L$ : the latent heat [ $J/kg$ ]

209  $R$ : heat transfer resistance's [ $s/m$ ]

210

211 In our model, the heat transfer resistance is a function of the convective  
212 heat transfer coefficient (Equation (6)). It is calculated from the correlation  
213 method with a characteristic length of 1m (for more detail see Azam et al.,  
214 2017 [16]). This method considers forced, mixed and natural convection.

$$R = \rho_{air} \cdot \frac{C_{p,air}}{h_c} \quad (6)$$

215

216  $C_{p,air}$ : air specific heat [ $J/kg/K$ ]

217  $h_c$ : the convective heat transfer coefficient [ $W/m^2/K$ ]

218

219 As the surface is impervious, the latent heat flux is only calculated when  
220 some water is present on the surface. This heat flux depends on the air  
221 characteristics (temperature, pressure, humidity and wind speed). The vapor  
222 pressure gradient is calculated between the air at a certain height and the  
223 saturated air very close to the water surface. The hypothesis is made that  
224 the saturated air very close to the water surface is at the same temperature  
225 than the water surface. The vapor pressure is calculated according to the  
226 Magnus-Tetens formulas (Alduchov and Eskridge, 1996 [26]) described by  
227 Equations (7), (8) and (9).

$$q_{sat} = 0.662 \frac{VP_{sat}}{101325 - 0.378 VP_{sat}} \quad (7)$$

$$q_a = 0.662 \frac{VP_{sat} \frac{RH}{100}}{101325 - 0.378 VP_{sat} \frac{RH}{100}} \quad (8)$$

$$VP_{sat} = 611.2 \exp\left(\frac{17.67 T}{243.5 + T}\right) \quad (9)$$

228  $VP_{sat}$ : saturated vapor pressure [ $Pa$ ]

229  $RH$ : Relative Humidity [%]

230



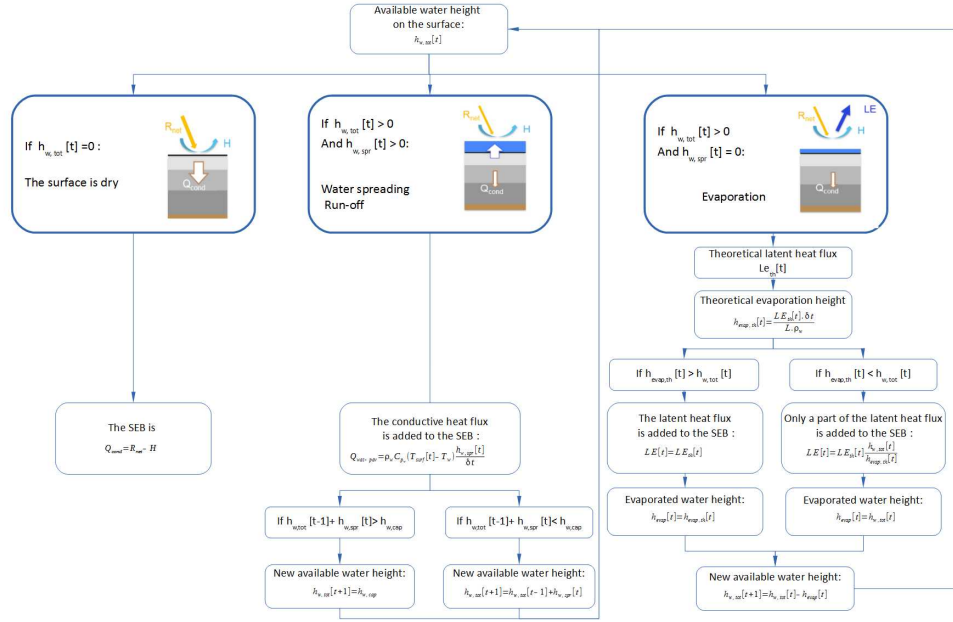


Figure 2: Flowchart of the surface energy balance calculation process for each step of a watering event.

#### 2.2.4. Heat fluxes dynamic

The Surface Energy Balance (hereafter denoted SEB) method is presented Figure 2. For each time step, the equivalent height of water that is evenly sprinkled on the surface is noted  $h_{w,spr}$ . The total height of water is noted  $h_{w,tot}$ . Then three cases are considered:

- $h_{w,tot}$  is equal to 0,
- $h_{w,tot}$  is higher than 0 and  $h_{w,spr}$  is higher than 0,
- or  $h_{w,tot}$  is higher than 0 but  $h_{w,spr}$  is equal to 0.

In the first case, the surface is dry then the conduction flux is simply defined as the difference between the global radiation flux and the sensible heat

241 flux. In the second case, water is sprinkled on the surface. We assume that  
242 no evaporation occurs at this time step. The energy is exchanged between  
243 the water and the ground. This convective heat flux is calculated consid-  
244 ering that the additional height of water  $h_{w,spr}$  reaches directly the surface  
245 temperature. Then a proportion of the total water height runs off decreasing  
246 the height of the water layer. The height  $h_{w,cap}$  of the water layer that re-  
247 mains at the surface depends on the water-holding capacity of the pavement.  
248 In the third case, the sprinklers are off some water remains on the surface.  
249 Only evaporation occurs and its potential is estimated and converted into an  
250 equivalent water height  $h_{evap,th}$ . If  $h_{w,tot}$  is higher than  $h_{evap,th}$ , the latent  
251 heat flux is equal to the evaporation potential. Else, the remaining height  
252  $h_{w,tot}$  is converted to an equivalent latent heat flux. The water height de-  
253 crease is equal to the evaporated water height. Then the next time step is  
254 considered.

### 255 **3. Model assessment**

256 The model is evaluated an open asphalt parking lot. The measurement  
257 campaign and the analysis of the watering event will be first presented (sec-  
258 tion 3.1). Then the model will be applied to this case and assessed (section  
259 3.2).

#### 260 *3.1. The campaign and the data*

##### 261 *3.1.1. Studied area and measurement description*

262 Data from the ROSURE/HydroVille experiment (Cohard et al., 2017  
263 [27]) are used to calibrate and evaluate the pavement watering model. The

264 experiment site is located near Nantes (France) and consisted of an asphalt  
265 car park of  $2500m^2$ . This campaign especially focused on surface and air  
266 temperatures and on heat flux measurement during a warm summer period  
267 (June 2004). During this experiment, the car park was watered by means of  
268 a set of artificial rain events (Figure 4).



Figure 3: View of the experimental site during a watering event (an asphalt parking lot of  $2500m^2$ )

269 Throughout the observations available for this campaign, this study fo-  
270 cused on the following variables, all observed in the middle of the car park:

- 271 ● surface and ground temperature: vertical profile at 0, 1, 2, 3, 4, 5, 6,  
272 10, 15, 24, 34, 50 and 75 cm depth;
- 273 ● wind speed and direction;
- 274 ● convective heat flux;
- 275 ● latent heat flux;

276 • radiation components.

277 The humidity and air temperature was measured outside from the car park.  
 278 The equipment used and their position is given in Figure 4. The data were  
 279 collected with a 1 min time step except for the sonic anemometer and the  
 280 KH20 Campbell Sci whose time step were 0.1 s. The final data were averaged  
 281 to 15 min time step.

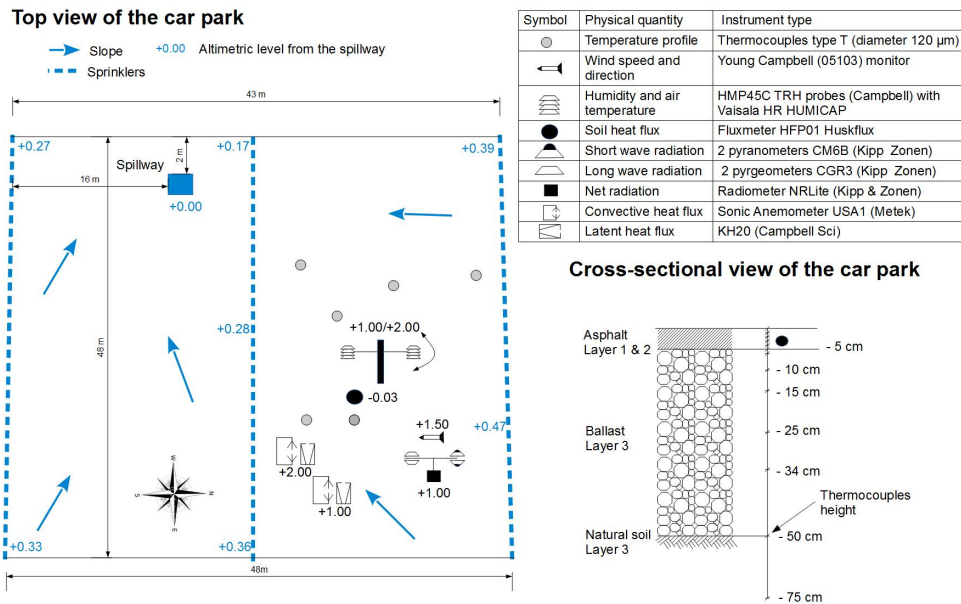


Figure 4: Top view of the car park with instruments approximate location during the campaign and cross-section of the soil composition (see Table 3 for the material properties)

282 *3.1.2. Description of the watering events*

283 16 watering events (including one natural event - the 15<sup>th</sup>) were recorded  
 284 during the entire measurement period (Figure 4). Each of them is described

<b>Watering</b>	<b>Date</b>	<b>Time</b>	<b>Total vol. of water</b>	<b>Intensity</b>	<b>Flow</b>
Number	DD/MM/YY HH:MM	minutes	$m^3$	$mm/m^2$	$m^3/h$
1*	02/06/04 13:42	20	16.96	6.78	43
2*	03/06/04 09:53	20	13.08	5.32	43
3*	03/06/04 15:04	20	15.05	6.02	44
4	04/06/04 08:49	3	2.04	0.81	44
5	04/06/04 11:57	1.5	1.12	0.45	44
6*	04/06/04 13:57	17	14.92	5.97	44
7	07/06/04 08:51	20	13.75	5.50	42
8	07/06/04 13:43	30	21.33	8.53	44
9	08/06/04 09:45	19	12.40	4.96	44
10	08/06/04 15:04	5	3.06	1.22	38
11	09/06/04 09:25	20	14.10	5.64	42
12	09/06/04 13:40	20	16.25	6.50	46
13	09/06/04 15:38	2	1.60	0.64	48
14	10/06/04 08:30	20	15.44	6.18	45
15	10/06/04 12:25	28	2.95	1.18	-
16	11/06/04 08:40	2	1.66	0.67	43

Table 1: Description of each watering event

285 in table 1. During the events numbered 1,2,3 and 6, some technical issues oc-  
286 curred and the total volume of water may be different from what is presented  
287 in Table 1. For each event, several parameters have been measured:

- 288 • inlet: water temperature, flow, and volume,
- 289 • outlet water temperature, flow, and volume,
- 290 • duration of each watering.

291 An indication is given on the approximate duration of the drying periods.

### 292 3.1.3. Consistency of the heat fluxes dynamics with the model assumptions

293 Sections 2.2.2 and 2.2.4, the assumption was made that energy is ex-  
294 changed between the runoff water and the surface only during the first time

295 step ( $t=15$  minutes). Then the latent heat flux is modelled. Those assump-  
 296 tions are here verified analysing the temperatures and heat flux measure-  
 297 ments.

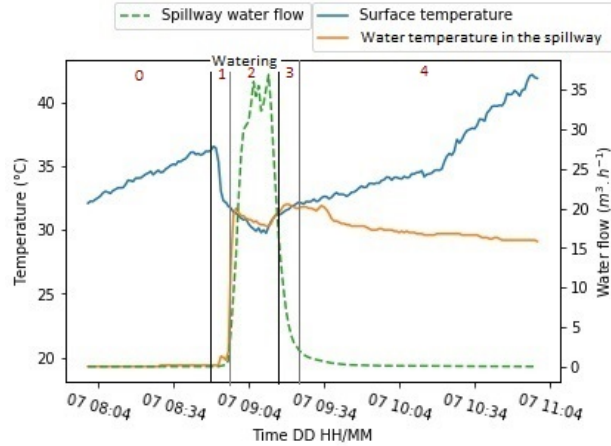


Figure 5: Watering event number 7, June 07<sup>th</sup> at 08:51am, measured surface temperature in the center of the parking lot and measured water temperature and water flow in the spillway

298 The surface temperature evolution is compared to the water temperature  
 299 and flow in the spillway in Figure 5. As soon as the watering event begins  
 300 (black line on Figure 5), the surface temperature drops and the water tem-  
 301 perature increases (zone 1 on Figure 5) until they reach a balance (grey line  
 302 on Figure 5). A delay of several minutes can be observed between the tem-  
 303 perature signals and the water flow signals (zone 1 and 3 on Figure 5). The  
 304 thermocouples are located at several meters from the spillway, as it can be  
 305 observed in Figure 4. The delay between the different signal is consistent  
 306 with the water travel time between the thermocouples location and the spill-  
 307 way. As the balance is reached, both temperatures increase (phase 3): no

308 more energy is exchanged between the surface and the water layer. As soon  
 309 as the water flow decreases (green plot), all the water has been drained. The  
 310 thermocouple now measures the temperature of the standing water in the  
 311 spillway, which slowly decreases (zone 4 on Figure 5).

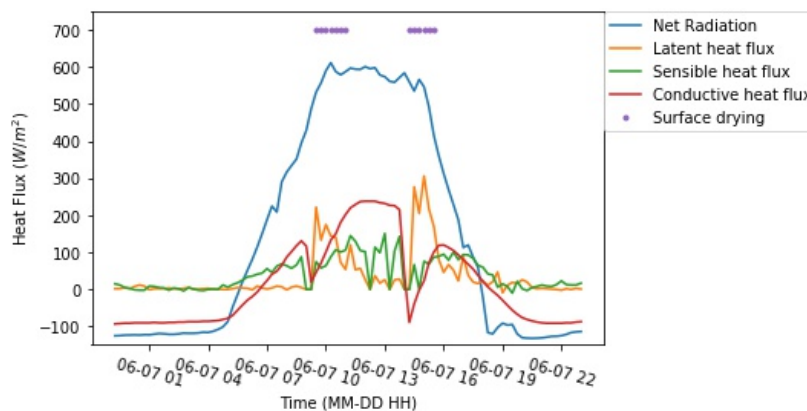


Figure 6: Observed surface energy balance (June 07<sup>th</sup>)

312 Those observations can be confronted with the heat fluxes measured pre-  
 313 sented in Figure 6. As said before the water temperature reaches very quickly  
 314 (less than 20 minutes) the surface temperature (Figure 5) whereas the con-  
 315 ductive heat flux in the ground has a decreasing peak right after watering  
 316 which then shrink in a short time (about one hour) (Figure 6). Cohard et  
 317 al (2017 [27]) also noticed a similar trend: the heat flux transferred from  
 318 the ground to the water can reach  $438W/m^2$  during a watering event and  
 319 decreases as soon as the sprinklers stop (15 minutes). Those observations are  
 320 consistent with the assumptions made for our modelling as well as the one  
 321 used by Herb et al. (2008 [18]): the run off convective heat flux exchanged  
 322 between the water and the surface can be attributed to the first time step  
 323 of the watering event. We assumed that air was saturated during the wa-

324 tering process and no evaporation occurred immediately. This assumption  
325 could not be verified in this measurement campaign since the latent heat flux  
326 sensor was protected when the sprinklers were working.

#### 327 *3.1.4. Water budget*

328 When some water is spread over a surface, a fraction runs off whereas  
329 the other fraction is intercepted by the surface until evaporation or infiltra-  
330 tion. The distribution of runoff and pavement storage depends on the surface  
331 water-holding capacity, itself related to the surface roughness. This charac-  
332 teristic is a parameter of the model that should be set by the user. The  
333 purpose of this part is to get an estimation of this parameter through the  
334 measurements of the water budget.

335 Cohard et al. (2017 [27]) estimated that for each watering event, a max-  
336 imum 0.1 and 0.2 mm of the height spread water infiltrates the ground. The  
337 water left over the surface is thus considered as entirely evaporated. To cal-  
338 culate the corresponding amount, they tested several methods derived from  
339 latent heat flux measurement or estimation. Their conclusion is that the la-  
340 tent heat flux estimated according to the SEB method (using measurements  
341 for the other fluxes values) was the most accurate. The results fitted with  
342 the water budget contrary to the other method used. They were then able to  
343 evaluate for each watering event the amount of water evaporated. For events  
344 with high volume of water (more than 2 mm), the mean evaporated height  
345 is 0.7mm. This value will be used as reference data for the evaluation of the  
346 model, and the water holding capacity will be calibrated in the model (see  
347 section 3.2.1).



Surface energy balance heat flux	Input data used to calculate each flux
Convective heat flux	wind speed air temperature*
Net radiative heat flux	Net radiative flux
Latent heat flux	water height water-holding capacity of the surface air relative humidity* air temperature*
Runoff convective heat flux	water temperature total sprinkled water for each event

\*measured outside from the watered zone of the car park

Table 2: Detail of each input data necessary to calculate the upper boundary condition.

### 3.2. Comparison between simulation and measurement

The model ability to properly reproduce the physical phenomenon related to a watering event is evaluated in this section. The model setup used are first presented, then the model is evaluated at several depths. Finally, as the soil model is proposed for different optimized grid distribution, the model sensitivity to the node distribution is studied.

#### 3.2.1. Model setup

The simulation is run for the whole period from June 5<sup>th</sup>, 00:00 to June 14<sup>th</sup>, 00:00, with a time step of 15 minutes. For the soil thermal model, a centimetric grid is used.

#### Surface energy balance:

The heat fluxes are calculated from the observed data presented in Table 2. The convective heat flux is calculated from the air temperature and the wind speed. Radiative heat fluxes are the observations. The latent

363 and run-off convective heat fluxes are calculated according to the processing  
 364 chain presented Figure 2. The runoff convective heat flux is calculated us-  
 365 ing the amount of water sprinkled during each watering event derived from  
 366 the measurement. The temperature of the sprinkled water is set at 18°C  
 367 before touching the ground. The latent heat flux is calculated from the air  
 368 characteristics measured outside from the watered zone.

369 **Thermal characteristics:**

370  
 371 The soil is composed of three different materials: 5cm-of asphalt, 45cm-  
 372 of ballast and an altered mica-schist natural soil underneath. Soil composi-  
 373 tion and thermal properties have not been measured during the campaign.  
 374 They have been calibrated according to the observed soil thermal profile,  
 375 reducing the difference between the measured and simulated surface temper-  
 376 ature, with a centimetric-grid. Data acquired on the 6<sup>th</sup> of June is used for  
 377 calibration. From the measured temperature gradient, changes in the soil  
 378 thermal properties within the first layer were identified (0–1 cm, 1–5 cm).  
 379 Values are gathered in Table 3.

Layer	Material	Depth	Thermal conduc-	Volumetric heat ca-
Number	Characteristics	m	tivity	capacity
			$W.m^{-1}.K^{-1}$	$10^6 J.m^{-3}.K^{-1}$
0	Asphalt Concrete	0.01	2.5	2.3
1	Asphalt Concrete	0.05	2.5	2.1
2	Old Filled Ballast	0.5	1.8	2.3
3	Altered Mica-schist Natural Soil	1	1.3	2.1

Table 3: Calibrated characteristics of the soil

380 **Water-holding capacity:**

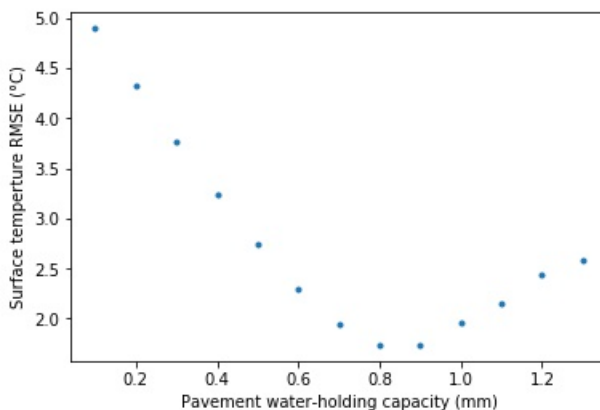


Figure 7: Surface temperature RMSE as a function of the pavement water-holding capacity (mm) for the calibration period (June, 7<sup>th</sup>, and 8<sup>th</sup>)

381

382 The water storage capacity of the surface may vary a lot depending on  
383 the surface type. To better evaluate this value for our studied area, the  
384 model has been run for two days from the 7<sup>th</sup> to the 8<sup>th</sup> of June (4 watering  
385 events), testing the water storage height from 0.3 to 1.4. The effect on the  
386 temperature surface RMSE is shown Figure 7. A water holding capacity of  
387 0.8 mm minimizes the surface temperature RMSE and then is used for the  
388 studied car park surface. Figure 8 presents the results of the calibration  
389 period and a minimum for a height of 0.8mm. The temporal variations are  
390 well reproduced (there is no phase lag between the signals) except during the  
391 watering events.

392 This value is consistent with mean evaporated height calculated from SEB  
393 method for a high amount of water (0.7 mm). In the literature Hendel et al.

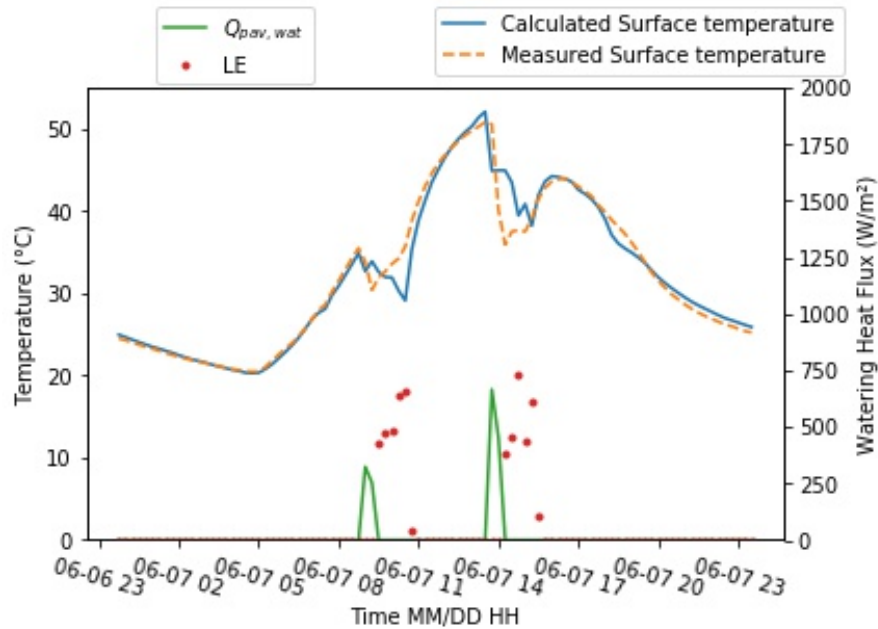


Figure 8: Comparison of simulated and measured temperatures at the surface for the calibration period (June, 7<sup>th</sup>, and 8<sup>th</sup>)

394 (2015 [7]) estimate to 1mm the water holding capacity of road surface in the  
 395 center of Paris. In TEB the default value is also set to 1 mm (Daniel et al.,  
 396 2016 [9]).

### 397 3.2.2. Watering model evaluation on ROSURE data

398 This paragraph deals with the evaluation of the model which is performed  
 399 by comparing the time series of observed and modelled surface temperatures  
 400 (Figure 9). Over the all data set, the temporal variations are well reproduced  
 401 (there is no phase lag between the signals) except during the watering events.  
 402 The same shape is obtained (a decreasing peak followed by more steady  
 403 period and then an increasing peak) but a lag is observed. This lag might

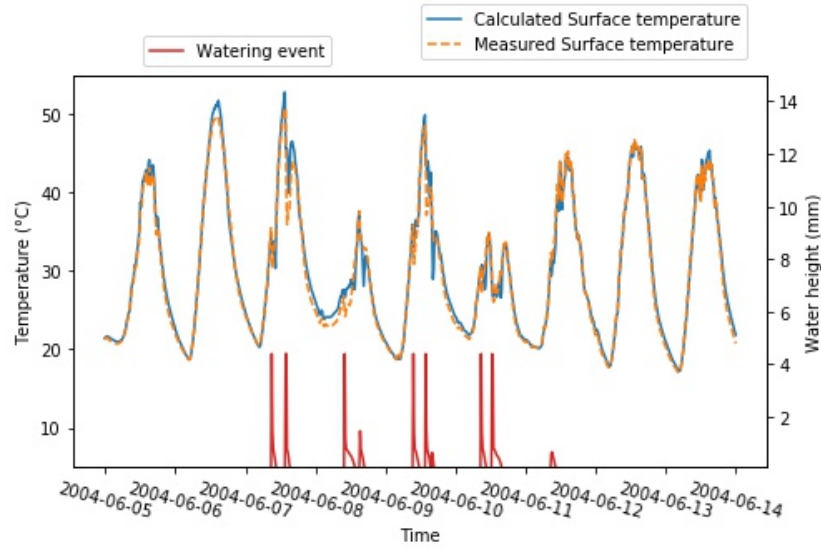


Figure 9: Comparison of simulated and measured temperatures at the surface from June, 5<sup>th</sup>, to 13<sup>th</sup>

404 have been attributed to the assumption that the drying stage does not start  
 405 as long as the sprinklers are in operation. To verify this assumption, we have  
 406 run some simulations starting the evaporation stage while sprinklers were  
 407 still working. The same temporal lag was noted and the simulated surface  
 408 temperature was lower than the observed one or the initial simulation. This  
 409 lag error could be attributed to the relative humidity measurement used  
 410 for the latent heat flux calculation. The sensor is located outside from the  
 411 sprinkled area and thus potentially underestimates the real relative humidity  
 412 of the air in the watered area. This results in an overestimation of the latent  
 413 heat flux which may affect the dynamic of the surface energy balance.

414 In order to determine the overall model performance, the RMSE between  
 415 estimated and observed temperatures is calculated at the surface and at sev-

Depth	RMSE ( $^{\circ}\text{C}$ )	RMSE ( $^{\circ}\text{C}$ )
	From June 8 <sup>th</sup> 23:45 to the 13 <sup>th</sup> 23:45 (soil + watering model)	From June 11 <sup>th</sup> 23:45 and 13 <sup>th</sup> 23:45 (soil model only)
Surface	1.04	0.71
5 cm	0.86	0.93
10 cm	0.66	0.78
34 cm	0.35	0.46
50 cm	0.21	0.29

Table 4: Evaluation of the centimetric grid watering model according to the experimental data

416 eral depths. To estimate the error which may be attributed only to the  
417 watering model, the RMSE is calculated for two different periods. The first  
418 period includes the entire campaign without the calibration days (from June  
419 9<sup>th</sup> to June 13<sup>th</sup>), whereas the second includes only two dry days (June 12<sup>th</sup>  
420 and 13<sup>th</sup>). The first set of RMSE assesses the overall model performance (soil  
421 and watering models) while the second RMSE set indicates the performance  
422 relative to the soil model only (ability to reproduce heat transfers into the  
423 ground). Results are presented in Table 4. The absolute RMSE for the sur-  
424 face temperature is larger when watering events are simulated ( $1.04^{\circ}\text{C}$ ) than  
425 when only the soil model is needed ( $0.71^{\circ}\text{C}$ ). For this specific dataset, the wa-  
426 tering model increased the soil model error of 46%. As the simulated days are  
427 not similar (weather condition are varying), this value is only representative  
428 for this specific simulation.

429 The assumption was made that the water-holding capacity of the surface  
430 was  $0.8\text{mm}$ . As it is an important parameter, the model is also evaluated on  
431 its ability to calculate the latent heat flux. For each event, the latent heat

Watering	Date	Duration	Total height of the water layer spread	Latent heat measured from SEB method	Latent heat calculated by the model	Relative error
Number	DD/MM/YY HH:MM	minutes	mm	$10^6 J$	$10^6 J$	%
7	07/06/04 08:51	20	5.50	2.11	1.96	-7.17
8	07/06/04 13:43	30	8.53	2.36	1.96	-17.04
9	08/06/04 09:45	19	4.96	2.00	1.96	-2.12
10	08/06/04 15:04	5	1.22	1.52	1.96	28.71
11	09/06/04 09:25	20	5.64	1.52	1.96	28.79
12	09/06/04 13:40	20	6.50	1.42	1.76	23.77
13	09/06/04 15:38	2	0.64	1.30	1.57	21.07
14	10/06/04 08:30	20	6.18	1.72	1.96	13.66
15	10/06/04 12:25	28	1.18	1.74	1.96	12.60
16	11/06/04 08:40	2	0.66	1.32	1.63	22.88

Table 5: Comparison of the latent heat flux estimated from SEB residue and calculated by the model. For each event, the latent heat fluxes are summed over the event duration.

432 fluxes calculated by the model and estimated from the SEB residual method  
433 are integrated over each event. The total energy due to evaporation for both  
434 methods is compared in table 5. The relative error stays below 29%. On  
435 average, the model overestimates the latent heat flux by 12%.

436 The air temperature and the relative humidity used to calculate the evap-  
437 oration were measured outside from the car park. If local parameters were  
438 used, an increase of the relative humidity and a decrease of the air temper-  
439 ature would have been observed. Then the calculated evaporation heat flux  
440 would have been smaller. The use of nonlocal meteorological data overesti-  
441 mates the latent heat flux calculation.

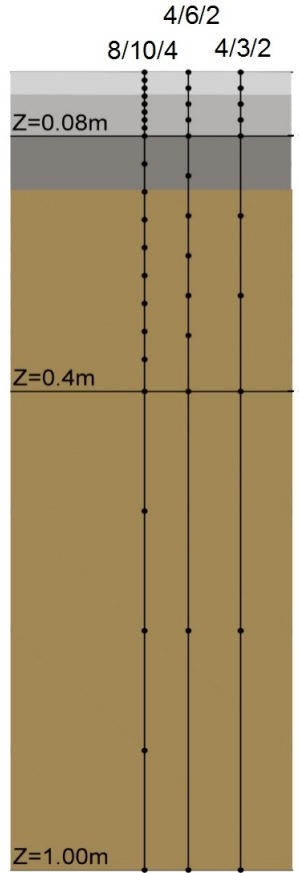


Figure 10: Description of the different grids

442 *3.2.3. Model's sensitivity to the discretization*

443 In order to reduce the simulation duration while keeping a reasonable  
 444 accuracy, three node distributions for the soil layer have been proposed in  
 445 Azam et al. (2017 [16]). They are presented in Figure 10. The sensitivity of  
 446 the model to this nodes distribution is here evaluated.

447 Figure 11 compares the surface temperature modelled with the three dif-  
 448 ferent node distribution with the measured one. Firstly, the three node distri-



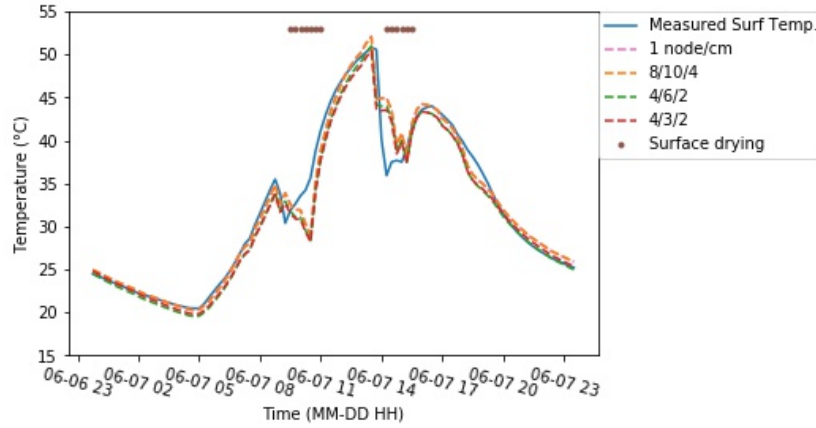


Figure 11: Surface temperature calculated with the different grids compared to that measured (June 7<sup>th</sup>)

449 butions allow an accurate modelling of the time series of surface temperature.  
 450 Nevertheless, the daily maximum and minimum peak are underestimated.

451 The underestimated daily maximum peak and minimum trough are due  
 452 to the heat fluxes implementation during watering events. However, the  
 453 reduction in the number of nodes deteriorates the results as it leads to dete-  
 454 riorate the representation of the heat transfer into the ground. In fact, this  
 455 induces a time shift of heat conduction, the main influence of which appears  
 456 when its sign changes.

457 The RMSE between simulated and observed surface temperatures is cal-  
 458 culated for each node distribution (Table 6). The accuracy loss due to the  
 459 reduction of the number of nodes is also evaluated calculating the RMSE of  
 460 the simulated surface temperature between each node distribution and the  
 461 centimetric grid (1 node per cm). The 8/10/4 grid has almost no effect on  
 462 the simulation performances (the RMSE increase is lower than 4%). The

Date	Reference data for RMSE calculation	Reference data for RMSE calculation			
		centimetric grid	grid 8/10/4	grid 4/6/2	grid 4/3/2
From June 8th 23:45 to the 13th 23:45 (soil + watering model)	observed temperature(°C)	1.04	1.04	1.44	1.50
	simulated temperature using centimetric grid (°C)	-	0.02	1.18	1.21
June 12th and 13th (soil model only)	observed temperature (°C)	0.70	0.72	1.10	1.20
	simulated temperature using centimetric grid (°C)	-	0.03	1.14	1.15

Table 6: Evaluation of the model with a reduced number of nodes

463 absolute RMSE increase due to the node distribution is almost similar re-  
464 gardless the models used (soil model only or soil model + watering model):  
465 0.02, 1.18, and 1.21 °C respectively for grids 8/10/4, 4/6/2 and 4/3/2. If  
466 we report these RMSE to the one due to the model itself (centimetric grid  
467 relative to the observed data), the relative accuracy loss due to the nodes  
468 distribution is much lower when the water model is taken into consideration.

#### 469 4. Conclusion

470 This article focuses on pavement watering as a possible mitigation tech-  
471 nique of the UHI effect under heat waves conditions. The literature review  
472 revealed that it technique has been mainly studied through experimental  
473 works. To the best of our knowledge, the impact of pavement watering on  
474 urban energy balance at the microscale has not yet been addressed by mod-  
475 elling.

476 The main purpose of this article was to implement a watering model  
477 within an urban microscale model (SOLENE-Microclimat) and to evaluate  
478 it according to an observation campaign.

479 The watering model was elaborated on a literature review and evaluated  
480 on an open asphalt car park. Two fluxes were taken into account: the runoff  
481 convective heat flux (exchanged between the surface and the runoff water)  
482 and the latent heat flux. The runoff convective heat flux is often neglected  
483 by existing models at mesoscale whereas the high difference of temperature  
484 between surface and the water spread makes it prevailing under heat wave  
485 conditions. In the case of the measurement campaign used to evaluate the  
486 model, the modelled heat flux represents 20% of the overall cooling flux  
487 ( $Q_{wat-pav} + LE$ ) due to the pavement watering.

488 The latent heat flux is limited by the water holding capacity of the pave-  
489 ment. This important parameter has been estimated using two methods: one  
490 based on simulation and the other based on the observation. The results are  
491 almost similar: the water holding capacity of the studied pavement is about  
492 0.8 mm, comparable to the 1 mm height found in the literature. The esti-  
493 mated latent heat flux is in average 12% higher than the observed one. The  
494 relative error never exceeds 30%. An explanation of this overestimation is  
495 that the relative humidity data used for the latent heat flux calculation was  
496 probably lower than the reality (the sensor was located outside the watered  
497 area).

498 The global accuracy of the model was evaluated using the temperature  
499 observed at the surface and at several depths. The absolute RMSE for the  
500 surface temperature is larger when watering events are simulated ( $1.04^{\circ}\text{C}$ )  
501 than under dry conditions when only the soil model is used ( $0.71^{\circ}\text{C}$ ).

502 The sensitivity of the model due to the node distribution has finally been

503 studied. Three soil model node distributions were compared. The 8/10/4  
504 grid has almost no effect on the simulation performances (the RMSE increase  
505 is lower than 4%).

506 This paper provides a detail evaluation of the watering model perfor-  
507 mances when compared with experimental data. This model can be used  
508 to assess the cooling induced by pavement watering mitigation technique at  
509 micro-scale, which was not possible until now. The impact on local comfort  
510 could then be estimated.

511 The efficiency of watering techniques is constrained by the surface po-  
512 tential evaporation which depends directly on the surface holding capacity.  
513 The model could then be used to optimize the watering scenario according  
514 to the surface characteristics of street. The impact of different materials on  
515 microclimat model could then be compared as porous surface.

## 516 **Acknowledgements**

517 This research work was carried out within the scope of the EVA Project,  
518 funded by the ADEME (French Environment and Energy Management Agency)  
519 under contract no. 1216C0037 and conducted in collaboration with Veolia  
520 2EI. The authors are grateful to the ADEME for its financial support, as  
521 well as to IFSTTAR, LHEEA, and ONEVU for providing us with the exper-  
522 imental data.

523 **References**

- 524 [1] J.-M. Robine, S. L. K. Cheung, S. Le Roy, H. Van Oyen, C. Griffiths, J.-  
525 P. Michel, F. R. Herrmann, Death toll exceeded 70,000 in europe during  
526 the summer of 2003, *Comptes rendus biologies* 331 (2008) 171–178.
- 527 [2] K. Laaidi, A. Zeghnoun, B. Dousset, P. Bretin, S. Vandentorren, E. Gi-  
528 raudet, P. Beaudeau, The impact of heat islands on mortality in paris  
529 during the august 2003 heat wave, *Environmental health perspectives*  
530 120 (2012) 254.
- 531 [3] S. Conti, P. Meli, G. Minelli, R. Solimini, V. Toccaceli, M. Vichi, C. Bel-  
532 trano, L. Perini, Epidemiologic study of mortality during the summer  
533 2003 heat wave in italy, *Environmental research* 98 (2005) 390–399.
- 534 [4] M. Santamouris, L. Ding, F. Fiorito, P. Oldfield, P. Osmond, R. Paolini,  
535 D. Prasad, A. Synnefa, Passive and active cooling for the outdoor built  
536 environment—analysis and assessment of the cooling potential of mitiga-  
537 tion technologies using performance data from 220 large scale projects,  
538 *Solar Energy* (2016).
- 539 [5] M. A. Hendel, M. Colombert, Y. Diab, L. Royon, Measurement of the  
540 cooling efficiency of pavement-watering as an urban heat island mitiga-  
541 tion technique, *Journal of Sustainable Development of Energy, Water  
542 and Environment Systems* 3 (2015) 1–11.
- 543 [6] S. Himeno, R. Takahashi, A. Asakura, K. Koike, S. Fujita, Using snow  
544 melting pipes to verify the water sprinkling s effect over a wide area,  
545 *NOVATECH 2010* (2010).

- 546 [7] M. Hendel, M. Colombert, Y. Diab, L. Royon, An analysis of pave-  
547 ment heat flux to optimize the water efficiency of a pavement-watering  
548 method, *Applied Thermal Engineering* 78 (2015) 658–669.
- 549 [8] A. M. Broadbent, A. M. Coutts, N. J. Tapper, M. Demuzere, The cooling  
550 effect of irrigation on urban microclimate during heatwave conditions,  
551 *Urban Climate* (2017).
- 552 [9] M. Daniel, A. Lemonsu, V. Vigiúé, Role of watering practices in large-  
553 scale urban planning strategies to face the heat-wave risk in future cli-  
554 mate, *Urban Climate* (2016).
- 555 [10] S. Grossman-Clarke, J. A. Zehnder, T. Loridan, C. S. B. Grimmond,  
556 Contribution of land use changes to near-surface air temperatures during  
557 recent summer extreme heat events in the phoenix metropolitan area,  
558 *Journal of Applied Meteorology and Climatology* 49 (2010) 1649–1664.
- 559 [11] C. Grimmond, M. Blackett, M. Best, J. Barlow, J. Baik, S. Belcher,  
560 S. Bohnenstengel, I. Calmet, F. Chen, A. Dandou, et al., The inter-  
561 national urban energy balance models comparison project: first results  
562 from phase 1, *Journal of applied meteorology and climatology* 49 (2010)  
563 1268–1292.
- 564 [12] V. Masson, A physically-based scheme for the urban energy budget in  
565 atmospheric models, *Boundary-layer meteorology* 94 (2000) 357–397.
- 566 [13] L. Malys, Évaluation des impacts directs et indirects des façades et des  
567 toitures végétales sur le comportement thermique des bâtiments, Ph.D.  
568 thesis, École nationale supérieure d’architecture (Nantes), 2012.

- 569 [14] M. Musy, L. Malys, B. Morille, C. Inard, The use of solene-microclimat  
570 model to assess adaptation strategies at the district scale, *Urban Climate*  
571 14 (2015) 213–223.
- 572 [15] J. Bouyer, Modelisation et simulation des microclimats urbains-Etude de  
573 l’impact de l’amenagement urbain sur les consommations energetiques  
574 des batiments, Ph.D. thesis, Universite de Nantes, 2009.
- 575 [16] M.-H. Azam, B. Morille, J. Bernard, M. Musy, F. Rodriguez, A new  
576 urban soil model for solene-microclimat: Review, sensitivity analysis  
577 and validation on a car park, *Urban Climate* (2017).
- 578 [17] S. Dupont, P. G. Mestayer, E. Guilloteau, E. Berthier, H. Andrieu,  
579 Parameterization of the urban water budget with the submesoscale soil  
580 model, *Journal of Applied Meteorology and Climatology* 45 (2006) 624–  
581 648.
- 582 [18] W. R. Herb, B. Janke, O. Mohseni, H. G. Stefan, Ground surface tem-  
583 perature simulation for different land covers, *Journal of Hydrology* 356  
584 (2008) 327–343.
- 585 [19] V. Singh, C. Xu, Evaluation and generalization of 13 mass-transfer equa-  
586 tions for determining free water evaporation, *Hydrological Processes* 11  
587 (1997) 311–323.
- 588 [20] C.-Y. Xu, V. Singh, Evaluation and generalization of temperature-based  
589 methods for calculating evaporation, *Hydrological processes* 15 (2001)  
590 305–319.

- 591 [21] T. Asaeda, V. T. Ca, The subsurface transport of heat and moisture  
592 and its effect on the environment: a numerical model, *Boundary-Layer*  
593 *Meteorology* 65 (1993) 159–179.
- 594 [22] Z. Qin, P. Berliner, A. Karnieli, Numerical solution of a complete surface  
595 energy balance model for simulation of heat fluxes and surface tempera-  
596 ture under bare soil environment, *Applied mathematics and computa-*  
597 *tion* 130 (2002) 171–200.
- 598 [23] H. Saito, J. Simunek, Effects of meteorological models on the solution of  
599 the surface energy balance and soil temperature variations in bare soils,  
600 *Journal of Hydrology* 373 (2009) 545–561.
- 601 [24] M. Best, A model to predict surface temperatures, *Boundary-Layer*  
602 *Meteorology* 88 (1998) 279–306.
- 603 [25] G. Mihalakakou, M. Santamouris, J. Lewis, D. Asimakopoulos, On the  
604 application of the energy balance equation to predict ground tempera-  
605 ture profiles, *Solar Energy* 60 (1997) 181–190.
- 606 [26] O. A. Alduchov, R. E. Eskridge, Improved magnus form approximation  
607 of saturation vapor pressure, *Journal of Applied Meteorology* 35 (1996)  
608 601–609.
- 609 [27] J. Cohard, J. Rosant, F. Rodriguez, H. Andrieu, P. Mestayer, P. Guille-  
610 vic, Energy and water budgets of asphalt concrete pavement under  
611 simulated rain events, *Urban Climate* (2017).